

Direct Identification of Amyloid Peptide Fragments in Human α -Synuclein Based on Consecutive Hydrophobic Amino Acids

Yongzhu Chen, Fei Peng, Tao Su, Hao Yang, and Feng Qiu*



Cite This: *ACS Omega* 2020, 5, 11677–11686



Read Online

ACCESS |



Metrics & More

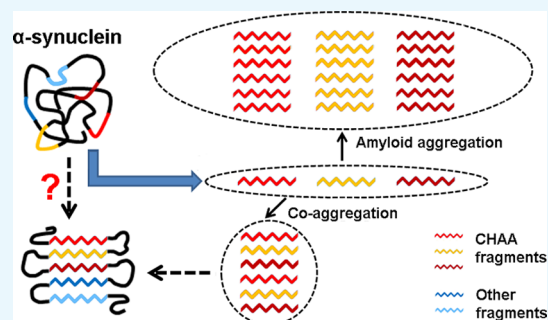


Article Recommendations



Supporting Information

ABSTRACT: Formation of amyloid fibrils by misfolding α -synuclein is a characteristic feature of Parkinson's disease, but the exact molecular mechanism of this process has long been an unresolved mystery. Identification of critical amyloid peptide fragments from α -synuclein may hold the key to decipher this mystery. Focusing on consecutive hydrophobic amino acids (CHAA) in the protein sequence, in this study we proposed a sequence-based strategy for direct identification of amyloid peptide fragments in α -synuclein. We picked out three CHAA fragments (two hexapeptides and one tetrapeptide) from α -synuclein and studied their amyloidogenic property. The thioflavin-T binding test, transmission electron microscopy, Congo red staining, and Fourier transform infrared spectroscopy revealed that although only hexapeptides could undergo amyloid aggregation on their own, extended



peptide fragments based on any of the three peptides could form typical amyloid fibrils. Primary amyloidogenic fragments based on the three peptides showed synergetic aggregation behavior and could accelerate the aggregation of full-length α -synuclein. It was proved that hydrophobic interaction played a predominant role for the aggregation of these peptides and full-length α -synuclein. A central alanine-to-lysine substitution in each hydrophobic fragment completely eliminated the peptides' amyloidogenic property, and alanine-to-lysine substitutions at corresponding sites in full-length α -synuclein also decreased the protein's amyloidogenic potency. These findings suggested that CHAA fragments were potentially amyloidogenic and played an important role for the aggregation of α -synuclein. The identification of these fragments might provide helpful information for eventually clarifying the molecular mechanism of α -synuclein aggregation. On the other hand, our study suggested that the CHAA fragment might be a simple motif for direct sequence-based identification of amyloid peptides.

INTRODUCTION

Amyloid fibrils formed by misfolding natural proteins or polypeptides have long been known as the hallmark of many human diseases including Alzheimer's disease, Parkinson's disease, type II diabetes, and so on.^{1,2} Understanding the molecular mechanism of how natural proteins or polypeptides misfold into amyloid fibrils holds the key to prevent, diagnose, and cure these diseases.³ On the other hand, formation of functional amyloid-like fibrils by natural proteins has attracted considerable attention in recent years, which also raised the challenge to decipher their aggregation mechanisms.⁴ However, despite worldwide effort for decades in this field, none of these amyloidogenesis processes has been fully understood from the molecular level. In addition, there is also a long-existing mystery about how different proteins with quite different sequences could form amyloid fibrils with very similar properties, such as a similar morphology and ability to bind with specific dyes.

Considering the complexity of full-length proteins or polypeptides, which are usually composed of tens to hundreds of amino acids, there is still a long way to clarify their precise molecular mechanisms of amyloid aggregation. For this reason, a rational strategy is to focus on amyloid peptide fragments in

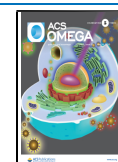
the proteins or polypeptides. These peptide fragments could self-assemble into amyloid fibrils by themselves and played determinative roles in the aggregation process of their full-length versions.⁵ In the past two decades, a number of amyloid peptide fragments have been identified from many different proteins or polypeptides, and a number of studies have been carried out on their aggregation behaviors and mechanisms, indicating a promising way to finally understand the mechanism of amyloid aggregation.^{6–10}

In order to identify amyloid peptides from natural proteins or polypeptides, various algorithms such as AMYLPRED and AGGRESCAN have been established to predict "aggregation-prone" fragments.^{11,12} In these algorithms, hydrophobicity of amino acids has been counted as a major positive index. Actually, nearly all literatures reported so far have indicated the

Received: March 4, 2020

Accepted: May 4, 2020

Published: May 12, 2020



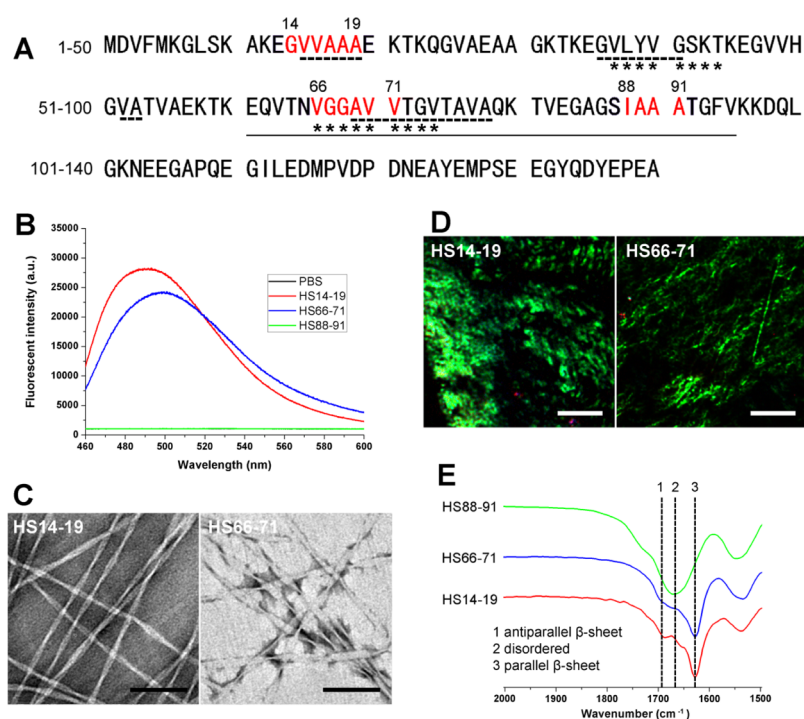


Figure 1. CHAA fragments and their amyloid aggregation behaviors. (A) Sequence of HS and selected CHAA fragments (red). Aggregation-prone fragments predicted by AMYLPRED are marked by dashed underlines. Experimentally confirmed amyloid peptides are marked by asterisks.^{27,28} Solid underline indicates the aggregation-prone NAC region. (B) ThT-binding fluorescence of CHAA fragments. (C) TEM images of helical nanotapes formed by HS14-19 and HS66-71. Scale bars = 100 nm. (D) Apple-green birefringence of HS14-19 and HS66-71 after CR staining. Scale bars = 50 μ m. (E) FT-IR spectra of CHAA fragments.

importance of hydrophobic amino acids in amyloid peptides.¹³ Based on these previous studies, we wonder if a simple criterion could be raised to identify amyloid peptides by directly checking their sequences for hydrophobic amino acids. Recently, we have found that a series of designer amphiphilic peptides could undergo amyloid-like aggregation when they contained fragments composed of at least four consecutive hydrophobic amino acids (CHAA).^{14,15} Coincidentally, many naturally derived amyloid peptides, such as KLVFFAE and GLMVGGVVIA from amyloid-beta peptide,^{16–18} NFGAILS and LANVFLVH from islet amyloid polypeptide,^{19,20} and RLQGGVLVNEI from the semen enhancer of HIV infection,²¹ also contained similar CHAA fragments. A detailed list of natural amyloid peptides containing similar CHAA fragments was summarized in Table S1. These findings implied that CHAA fragments might be a potential type of the amyloidogenic motif, which could serve as a simple criterion for identifying amyloid peptides from natural proteins.

Human α -synuclein (HS) is one of the most widely investigated amyloid proteins with its misfolding behavior strongly related to Parkinson's disease.^{22–24} To date, a lot of research studies have been carried out on the aggregation behavior of HS, and it has been known that among its sequence composed of 140 amino acids, the non- β -amyloid component (NAC) sequence (residues 61–95) rich in hydrophobic amino acids is the core region responsible for aggregation.^{25,26} Although a sketchy model has been proposed to illustrate how HS underwent amyloid aggregation based on several β -sheet-forming fragments,¹³ only a few amyloid peptide fragments have been identified from this protein, leaving the majority of its amyloidogenic fragments unexplored.^{27–29} As more and more studies suggested that the

architecture of HS amyloid fibrils might hold the key to manipulate its neurotoxicity and infectivity,^{30,31} a precise misfolding model based on more well-evaluated amyloid peptide fragments is highly demanded.

In order to identify more amyloid peptide fragments from HS and also to confirm our hypothesis that the CHAA fragment was a potential amyloidogenic motif, we picked out two hexa-CHAA fragments and one tetra-CHAA fragment from HS. In this study, we reported the amyloidogenic property of these fragments and showed their important role in the aggregation process of full-length HS.

RESULTS AND DISCUSSION

Selection and Analysis of CHAA Fragments. Based on the hydropathy index of amino acids developed by Kyte and Doolittle, G, A, M, C, F, L, V, and I were defined as hydrophobic amino acids in this study.³² In the sequence of HS, there are three CHAA fragments composed of at least four amino acids, that is, HS14-19 (GVVAAA), HS66-71 (VGGAVV), and HS88-91 (IAAA). As shown in Figure 1A, HS14-19 contained an aggregation-prone fragment predicted by AMYLPRED, a consensus method based on several different algorithms,¹¹ but no amyloid peptide around this region has been experimentally confirmed. HS66-71 partially overlapped with another aggregation-prone fragments predicted by AMYLPRED, and it is also the truncated version of an experimentally confirmed amyloid peptide.²⁸ On the other hand, no predicted or experimentally confirmed amyloid peptide around HS88-91 has been reported. Furthermore, it should be noted that HS66-71 and HS88-91 were from the NAC region of HS, while HS14-19 was from the N-terminal

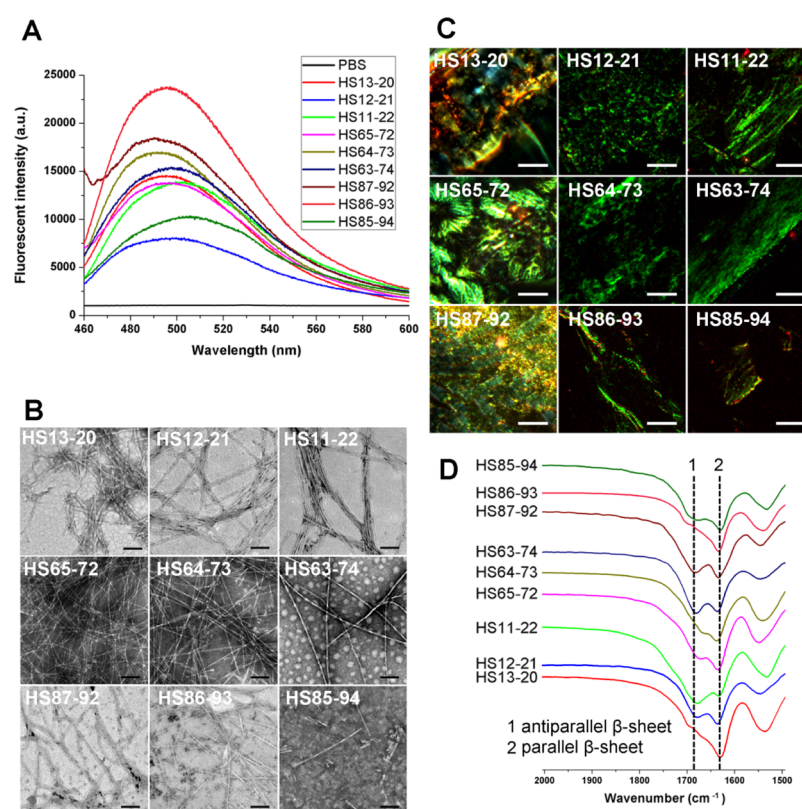


Figure 2. Amyloid aggregation of extended peptides containing CHAA fragments. (A) ThT-binding fluorescent spectra of different peptides. (B) TEM images of nanofibers formed by different peptides. Scale bars = 100 nm. (C) Apple-green birefringence of different peptides after CR staining. Scale bars = 50 μm. (D) FT-IR spectra of different peptides.

region, the amyloidogenic potency of which has not been well acknowledged yet.

Amyloid Aggregation of CHAA Fragments. The aggregation property of the three CHAA fragments was first evaluated by thioflavin-T (ThT) binding, a conventional method detecting amyloid aggregates in solution.^{33,34} As shown in Figure 1B, HS14-19 and HS66-71 exhibited a characteristic fluorescent peak around 495 nm, suggesting the formation of amyloid aggregates. On the contrary, the fluorescent spectrum of HS88-91 almost overlapped with that of the PBS control, indicating that the peptide did not undergo aggregation. TEM images showed that both HS14-19 and HS66-71 self-assembled into helical nanotapes (Figure 1C) while HS88-91 did not form any nanostructure (data not shown). Although the nanotapes formed by HS14-19 and HS66-71 did not resemble the morphology of typical amyloid fibrils, similar nanotapes formed by other amyloid peptides have also been reported,^{35,36} representing a special type of amyloid aggregates. Additionally, deposits of HS14-19 and HS66-71 stained by Congo red (CR) showed apple-green birefringence under polarized light (Figure 2D), which is also a well-known feature of amyloid aggregates.³⁷ Finally, as shown in Figure 1E, Fourier transform infrared (FT-IR) spectra of HS14-19 and HS66-71 exhibited amide-I peak around 1625–1630 and 1680–1690 cm⁻¹, indicating the formation of the parallel β-sheet and antiparallel β-sheet, respectively.^{38,39} On the contrary, the amide-I peak of HS88-91 appeared around 1660–1700 cm⁻¹, suggesting that the peptide took a disordered secondary structure. In combination, these results indicated that the selected hexa-CHAA fragments HS14-19 and HS66-71 could undergo amyloid aggregation while the

tetra-CHAA fragment HS88-91 could not, suggesting that four hydrophobic amino acids might not be long enough to support self-assembly on its own.

Amyloid Aggregation of Extended Peptides Containing CHAA Fragments. Then, the three CHAA fragments were extended on both of their N-terminal and C-terminal by 1–3 amino acids according to corresponding sequences in HS, and aggregation behaviors of these extended peptides were studied. As shown in Figure 2A, all extended peptides containing CHAA fragments, even including those containing nonamyloidogenic HS88-91, exhibited specific ThT-binding fluorescence with a peak value around 495 nm, indicating their potential amyloid aggregation potency. To compare the amyloidogenic potency of CHAA motifs and their extended fragments, the peak fluorescent value of different peptides were also shown in Figure S1. TEM images confirmed that all extended peptides self-assembled into nanofibers with a morphology similar to typical amyloid fibrils (Figure 2B). After CR staining, all extended peptides exhibited apple-green birefringence under polarized light, which further confirmed their amyloid property (Figure 2C). As shown in Figure 2D, FT-IR spectra of all extended peptides showed the amide-I peak around 1625–1630 and 1680–1690 cm⁻¹, indicating the formation of the parallel β-sheet and antiparallel β-sheet, respectively.

In combination, these results suggested that extended peptides containing CHAA fragments could also undergo amyloid aggregation. This is not surprising for peptides based on HS14-19 and HS66-71 because the core sequences they contained were amyloidogenic. A similar pattern has been very common in designer functionalized self-assembling peptide

nanofibers, in which self-assembling core sequences were responsible for self-assembly, and additional functional sequences would not affect the self-assembling behavior.^{40–43} Interestingly, although the primary amyloid peptides HS14-19 and HS66-71 formed nanotapes, all their extended versions formed nanofibers similar to amyloid fibrils formed by full-length HS protein, suggesting that extended peptides mimicked the aggregation behavior of HS more closely. Previous studies have suggested that peptides with shorter sequence or more hydrophobic terminal groups tended to form sheet-like or tape-like structures rather than nanofibers,^{44,45} and this might explain the special morphology of nanotapes formed by HS14-19 and HS66-71. However, more studies are needed to demonstrate the exact mechanism behind.

Surprisingly, although HS88-91 did not undergo amyloid aggregation as shown in Figure 1, all of its extended versions showed aggregation ability. Compared with the HS88-91 fragment, HS87-92 with additional S and T had an extended peptide backbone, which provided possibility for stronger intermolecular attraction. For example, in HS88-91 there were only three amide groups while in HS87-92 there were five, so that HS87-92 contained two more sites for stronger intermolecular hydrogen bonds. On the other hand, although S and T were generally classified as hydrophilic amino acids, they were uncharged so that would not generate electrostatic repulsion and weaken the hydrophobic interaction among the CHAA fragments, which also facilitated the self-assembling process. Furthermore, the methyl group in the side chain of T might also contribute to the overall hydrophobicity of the peptide. Possibly for these reasons, HS87-92 became the primary fragment capable of amyloid aggregation in the group of peptides based on HS88-91.

A summary of the aggregation ability of all CHAA fragments and extended peptides based on them is listed in Table 1.

Table 1. Sequence and Aggregation Ability of CHAA Fragments and Extended Peptides Based on Them

peptide	sequence ^a	type of amyloid aggregate
HS14-19	<u>GVVAAA</u>	nanotape
HS13-20	<u>EGVVAAAE</u>	nanofiber
HS12-21	<u>KEGVVAAAEK</u>	nanofiber
HS11-22	<u>AKEGVVAAAEKT</u>	nanofiber
HS66-71	<u>VGGAVV</u>	nanotape
HS65-72	<u>NVGGAVVT</u>	nanofiber
HS64-73	<u>TNVGGAVVTG</u>	nanofiber
HS63-74	<u>VTNVGGAVVTGV</u>	nanofiber
HS88-91	<u>IAAA</u>	no aggregate
HS87-92	<u>SIAAAT</u>	nanofiber
HS86-93	<u>GSIAAATG</u>	nanofiber
HS85-94	<u>AGSIAAATGF</u>	nanofiber

^aUnderlines indicate CHAA fragments.

Synergetic Aggregation and Seeding Effect of Primary Amyloid Peptides. Because HS14-19, HS66-71, and HS87-92 were identified as primary fragments capable of amyloid aggregation, we further studied their synergetic co-aggregation behavior, which could provide clue about how full-length HS could undergo amyloid aggregation based on these different fragments. As shown in Figure 3A, at lower concentration of 0.5 mM, HS14-19, HS66-71, or HS87-92 alone only showed slightly increased ThT-binding fluorescence, indicating an initial state of amyloid aggregation.

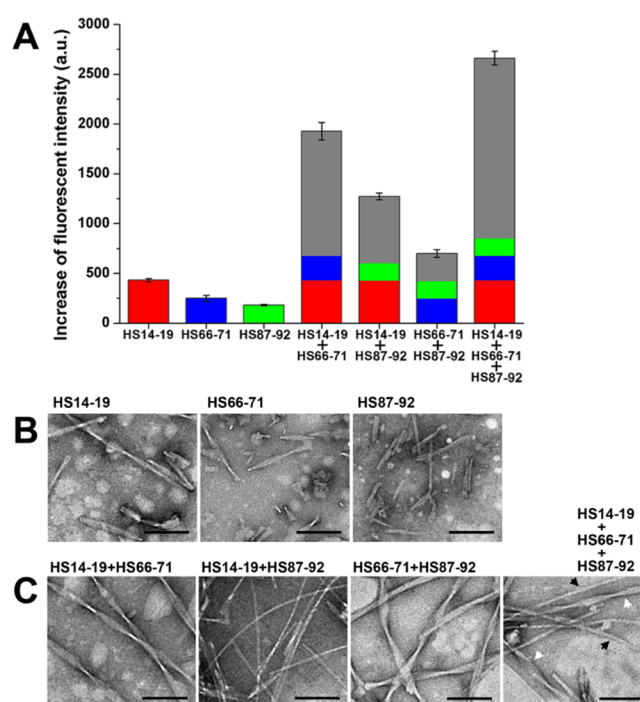


Figure 3. Co-aggregation of HS14-19, HS66-71, and HS87-92. (A) Increased ThT-binding fluorescence at 495 nm of different peptides and their combinations. For each sample, an increased fluorescent intensity was calculated by subtracting the value in PBS from the value in peptides. (B) TEM images of fragmental aggregates formed by different peptides. Scale bars = 100 nm. (C) TEM images of intact aggregates formed by different combination of different peptides. In the last image, black arrows indicate nanofibers, and white arrows indicate helical nanotapes. Scale bars = 100 nm.

However, in different combinations of different peptides, the increased values of ThT-binding fluorescence were much higher than the sum of increased values of corresponding peptides, indicating the synergetic aggregation behavior of different primary amyloid peptides.

Corresponding to the increase of ThT-binding fluorescence, as shown in Figure 3B, TEM images revealed that HS14-19 or HS66-71 only formed short fragments of helical nanotapes, and HS87-92 only formed short nanofibers. It should be pointed out that even these fragmental nanostructures were hard to find under TEM, suggesting immature and unstable self-assembly of these peptides at lower concentration. As shown in Figure 3C, when these peptides were mixed together at the same concentration, they could co-assemble into intact and stable nanostructures. Because both HS14-19 and HS66-71 formed helical nanotapes on their own, it is not surprising that their combination also formed helical nanotapes. Interestingly in other binary combinations, HS14-19 seemed to join in HS87-92 to form nanofibers while HS87-92 seemed to join in HS66-71 to form nanotapes. Also, in the combination of all the three peptides, both nanotapes and nanofibers were formed. It is not clear why would certain peptides take the predominant role in determining the morphology of co-assembling systems, but these TEM images also confirmed the co-aggregation behavior of different peptides. This synergetic co-aggregation manner also agreed well with the previously proposed aggregation model of HS, in which different potential amyloidogenic β -sheet fragments stacked with each other and formed amyloid aggregates.¹³

Except for co-aggregating with each other, these primary amyloid peptides could also induce the aggregation of full-length HS. As shown in Figure 4, agitated HS solution

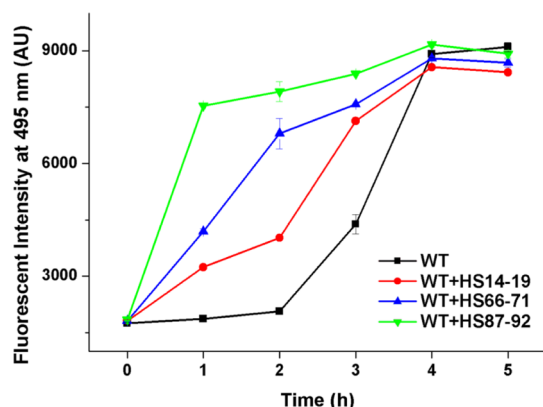


Figure 4. Growth of ThT-binding fluorescence of HS incubated with preformed aggregates of different peptides.

experienced a 2-day lag phase before the formation of amyloid aggregates. However, when amyloid aggregates preformed by each peptide added into HS solution, the protein began to aggregate from the first day, indicating the seeding effect of these primary amyloid peptide fragments.

Hydrophobic Interaction for Aggregation. Because these peptides could undergo similar amyloid aggregation and could readily undergo co-aggregation, they should share a common aggregation mechanism under a common driving force. Because all these peptides contained CHAA fragments as their major component, it is highly possible that hydrophobic

interaction as a common driving force played a predominant role for their aggregation behavior. To prove this, we first used pyrene and 8-anilinoanthracene-1-sulfonic acid (ANS) as probes to detect the formation of hydrophobic interaction in the self-assembling structure of each peptide. Pyrene is a hydrophobic molecular probe with five characteristic fluorescent peaks between 360 and 440 nm when excited at 336 nm. When the probe is in a hydrophobic environment, the ratio between its first peak (I_1) and third peak (I_3), that is, the I_1/I_3 value would drop significantly. As shown in Figure 5A, in all peptides except HS88-91, the I_1/I_3 value of pyrene decreased significantly as compared with pyrene in the PBS control, suggesting the formation of the hydrophobic region in all these amyloid peptides. Alternatively, ANS is another fluorescent probe used for detecting hydrophobic interaction by the enhancement and the blueshift of its fluorescent peak. As shown in Figure 5B, except HS88-91, all peptides showed an obviously enhanced and blue-shifted ANS fluorescent peak, which also confirmed the formation of hydrophobic interaction in all amyloid peptides.

Because hydrophobic interaction was supposed to be a crucial driving force for the peptides' amyloid aggregation, we further tested their aggregation potency in the mixture of PBS and tetrahydrofuran (THF). Compared with water, THF is a more hydrophobic solvent, so that it may bind with hydrophobic face of proteins or peptides, which might inhibit their aggregation by disturbing the intermolecular hydrophobic interaction directly or by perturbing the structure of protein or peptide monomers.^{46,47} As shown in Figure 5C, aggregation ability of all amyloid peptides was significantly inhibited by THF in a concentration-dependent manner, suggesting the importance of hydrophobic interaction in the aggregation

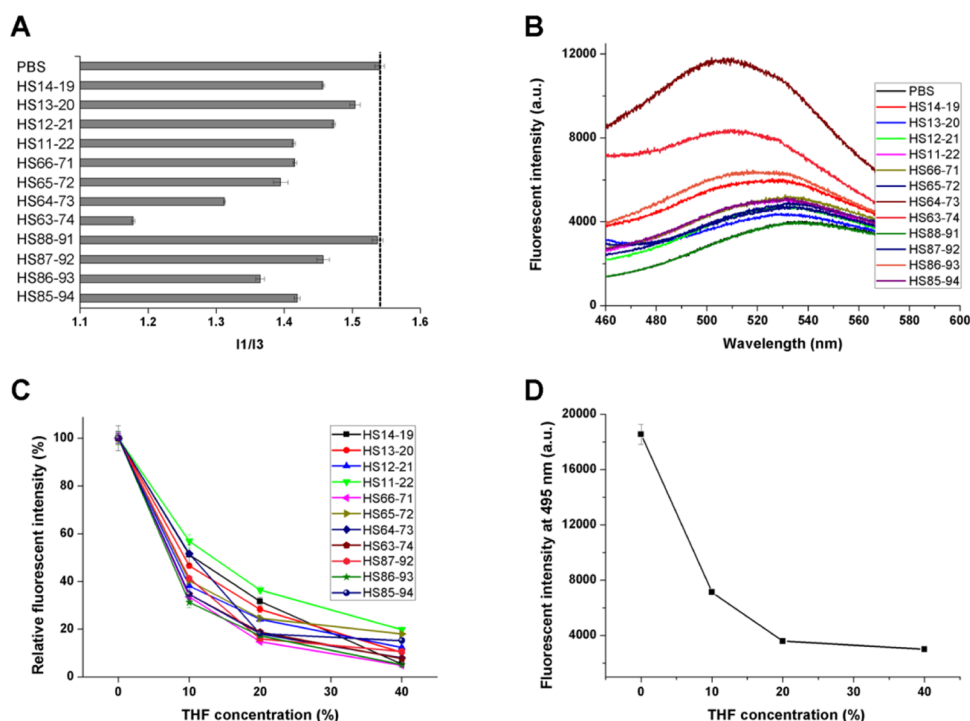


Figure 5. Role of hydrophobic interaction for amyloid aggregation. Both the I_1/I_3 value of pyrene fluorescent spectra (A) and ANS fluorescent spectra (B) revealed the existence of hydrophobic interaction in different amyloid peptides. (C) Relative ThT-binding fluorescent intensity at 495 nm of different peptides in the PBS/THF mixture with different THF concentrations. (D) ThT-binding fluorescent intensity of fibrillated HS in PBS/THF mixture with different THF concentrations.

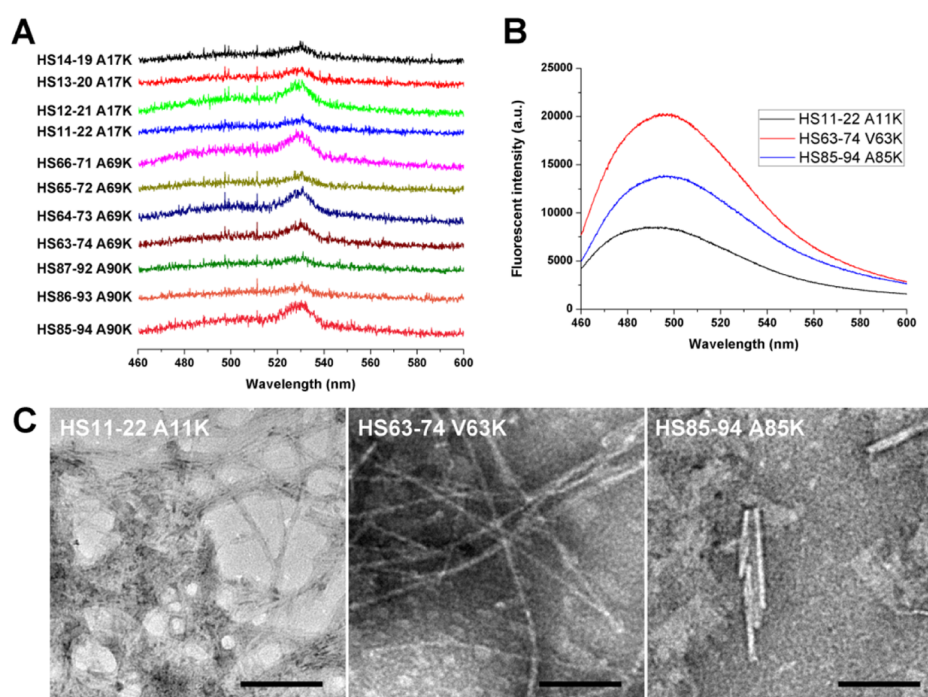


Figure 6. Aggregation of peptides with alanine-to-lysine substitution. (A) ThT-binding fluorescence of peptides with substitution at the center of CHAA motifs. (B) ThT-binding fluorescence of peptides with substitution at the N-terminal. (C) TEM images of nanofibers formed by peptides with N-terminal substitution. Scale bars = 100 nm.

process. Furthermore, we also tested the effect of THF on preformed aggregates of full-length HS. As shown in Figure 5D, as the concentration of THF increased, aggregates formed by HS was gradually destroyed, suggesting that the protein's aggregation also greatly relied on hydrophobic interaction. On the one hand, these results proved that hydrophobic interaction based on CHAA fragments played a predominant role for amyloid aggregation of HS, providing important clue for clarifying the protein's aggregation mechanism. On the other hand, although THF is highly toxic and may not be a good candidate drug for Parkinson's disease, other small molecules could be exploited to destroy amyloid aggregates with the same mechanism.

Effect of Alanine-to-Lysine Substitution on Aggregation. In order to eliminate the amyloid aggregation behavior of peptides by weakening hydrophobic interaction, a more direct strategy is to substitute hydrophobic amino acid in the sequence with hydrophilic acid. Because it was supposed that CHAA fragments were crucial for amyloid aggregation, we modified the CHAA-containing peptides by substituting one of their central alanines to lysine to destroy the continuity of CHAA motifs. As shown by ThT-binding fluorescence, alanine-to-lysine substitution in the center of CHAA fragments completely eliminated aggregation ability of all peptides based on them (Figure 6A), suggesting that continuity of hydrophobicity in the CHAA fragments was indispensable for all these peptides' aggregation.

As a comparison, we also tested the effect of terminal hydrophobic-to-hydrophilic substitution on the peptides' aggregation. As shown in Figure 6B,C, when the N-terminal alanines of HS11-22 and HS85-94, or N-terminal valine of HS64-73 were substituted with lysine, all modified peptides retained their amyloid aggregation ability and self-assembled into nanofibers. These results further demonstrated that a central CHAA fragment with restricted continuity was

indispensable for the aggregation of peptides, while the hydrophobicity of terminal amino acids was less important. A summary of the aggregation ability of all peptides with alanine-to-lysine substitution (valine-to-lysine for HS63-74 V63K) was listed in Table 2.

Table 2. Sequence and Aggregation Ability of Peptides with Alanine-to-Lysine Substitution

peptide	sequence ^a	type of amyloid aggregation
HS14-19 A17K	G <u>V</u> VKAA	no aggregation
HS13-20 A17K	EGV <u>V</u> KAAE	no aggregation
HS12-21 A17K	KEGV <u>V</u> KAAEK	no aggregation
HS11-22 A17K	AKEGV <u>V</u> KAAEKT	no aggregation
HS11-22 A11K	<u>K</u> KEGVVAAA <u>E</u> KT	nanofibers
HS66-71 A69K	VGG <u>K</u> VV	no aggregation
HS65-72 A69K	NVGG <u>K</u> VVT	no aggregation
HS64-73 A69K	TNVGG <u>K</u> VVTG	no aggregation
HS63-74 A69K	VTNVGG <u>K</u> VVTGV	no aggregation
HS63-74 V63K	<u>K</u> TNVGGAVVTGV	nanofibers
HS87-92 A90K	SIA <u>K</u> AT	no aggregation
HS86-93 A90K	GSI <u>A</u> KATG	no aggregation
HS85-94 A90K	AGSIA <u>K</u> ATGF	no aggregation
HS85-94 A85K	<u>K</u> GSIAAATGF	nanofibers

^aUnderlines indicate the site of substitution.

Based on these results, we wonder if corresponding alanine-to-lysine substitutions in full-length HS could also eliminate its amyloid aggregation ability. We constructed mutant HS proteins with a single alanine-to-lysine substitution at A17, A69, or A90, which was corresponding to the central alanine substitution in HS14-19, HS66-71, and HS88-91, respectively. Another mutant protein with all three alanines substituted by lysines was also constructed. These mutant proteins were named as Mut-A17K, Mut-A69K, Mut-A90K, and Mut-tri,

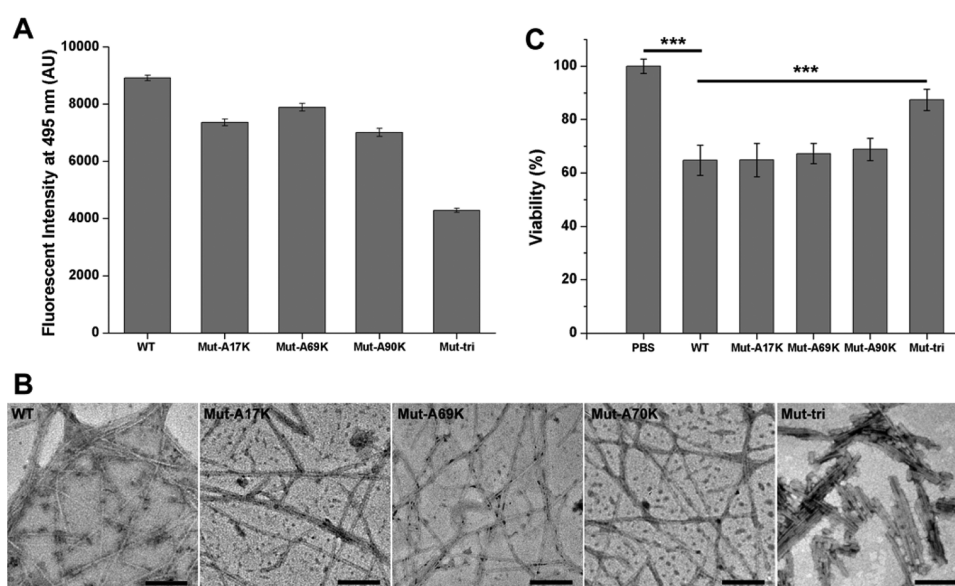


Figure 7. Aggregation and cytotoxicity of mutant HS proteins with alanine-to-lysine substitution. (A) ThT-binding fluorescence of proteins with different substitutions. (B) TEM images of amyloid fibrils formed by proteins with different substitutions. Scale bars = 100 nm. (C) Viability of PC12 cells incubated with amyloid fibrils formed by proteins with different substitutions. *** $P < 0.001$, $n = 4$.

respectively, and their aggregation potency was investigated. As shown in Figure 7A, although single alanine-to-lysine substitution only slightly decreased the ThT-binding fluorescence of Mut-A17K, Mut-A69K, and Mut-A90K, Mut-tri showed significantly decreased ThT-binding fluorescence. Correspondingly, TEM images showed that Mut-A17K, Mut-A69K, and Mut-A90K formed typical amyloid fibrils with a morphology similar to that formed by the WT protein, while Mut-tri formed much shorter nanofibers (Figure 7B). Furthermore, as shown in Figure 7C, although single alanine-to-lysine substitution at the central site of one of these CHAA fragments had no obvious effect on the cytotoxicity of Mut-A17K, Mut-A69K, and Mut-A90K, the cytotoxicity of Mut-tri was significantly lower than that of the WT protein.

Just as the CHAA fragments could undergo co-assembly in a synergetic manner, modifying these fragments to inhibit amyloid aggregation of HS also showed an accumulative effect. These results suggested that amyloid aggregation of HS was determined by the co-aggregation of all these different CHAA fragments, while the effect of a single mutation was limited. On the other hand, it should be noticed that even Mut-tri containing all three alanine-to-lysine substitutions still retained certain ability of amyloid aggregation and cytotoxicity, suggesting that the three CHAA fragments identified in our study were not fully responsible for amyloid aggregation of HS. This is not surprising because other amyloid peptide fragments from HS have also been reported earlier,^{27–29} and CHAA may not be the only motif capable of amyloid aggregation.

CONCLUSIONS

In conclusion, we have directly identified three CHAA fragments from HS based on the hydrophobicity of amino acids and proved the important role of these CHAA fragments for amyloid aggregation of the protein. Although HS66–71 partially overlapped with previously reported amyloid peptides from HS, HS14–19, and HS88–91 were new amyloid peptide fragments confirmed in this protein. More interestingly, HS14–19 was picked out from the N-terminal region of HS,

suggesting that the role of this region in aggregation should not be ignored. Although these CHAA fragments were only partially responsible for the aggregation of HS, our results expanded the family of amyloid peptides in HS, which might be helpful to finally clarify the protein's misfolding mechanism. Furthermore, although CHAA may not be the only type of motif capable of amyloid aggregation, our findings could also provide useful clue to identify more critical amyloid peptides from other proteins related to human diseases.

METHODS

Prediction of Amyloid Peptides by AMYLPRED. Amino acid sequence of human α -synuclein in one-letter code was inputted online (<http://aias.biol.uoa.gr/AMYPRED/>) and predicted for potential amyloid peptides by AMYLPRED.¹¹

Peptide Samples and Reagents. All peptides used in this study were purchased from Shanghai Bootech BioScience & Technology Co., Ltd (Shanghai, China) as lyophilized powder with purity over 95%. Each peptide was dissolved in phosphate buffer saline (PBS) as 5 mM stock solution and stored at room temperature (RT). Peptide samples with concentrations of 1 mM or 0.5 mM as well as the mixture of different peptides with concentration of 0.5 mM were prepared from the stock solutions, treated by ultrasound for 30 min, and incubated at RT for 24 h before experiments. All chemical reagents including ThT, CR, pyrene, ANS, and THF were purchased from Sigma-Aldrich Co. (St Louis, MO, USA).

ThT-Binding Assay. ThT powder was dissolved in Milli-Q water as 1 mM stock solution. For ThT-binding assay, each 500 μ L of peptide or protein sample was mixed with 5 μ L of ThT stock solution, incubated in dark at RT for 5 min, and the fluorescent spectrum was collected with a Fluorolog spectrometer (HORIBA Ltd, Kyoto, Japan). An excitation wavelength was set to 450 nm, and emission wavelength was set between 460 and 600 nm. In case the peak value around 495 nm was needed, each sample was measured for three times to get an averaged value.

TEM Observation. For TEM observation, 20 μL of each peptide or protein solution was set on a copper grid covered by Formvar and carbon films for 2–3 min to deposit the sample, and excess liquid was blotted with filter paper. After that 20 μL of 2% phosphotungstic acid was dropped onto the grid to stain the sample for 2–3 min, and excess liquid was blotted with filter paper. Finally the grid was air-dried and observed with TEM (Tecnai G2 F20, FEI, USA).

CR Staining. CR staining solution was prepared by saturating CR powder in 80% ethanol and pass through 0.22 μm filter. For CR staining, 50 μL of each peptide solution was dropped onto a glass slide and air-dried, and then 100 μL of CR staining solution was dropped onto the peptide sample to stain it for 5 min, after which the slide was gently rinsed with Milli-Q water and air-dried. A DM4000 B microscope (Leica Microsystems, Ltd., Germany) equipped with a polarizing stage was used to observe the stained sample under polarized light.

Fourier Transform Infrared. For FT-IR spectra measurement, 2 mL of each peptide solution (1 mM) was condensed to dry powder in a vacuum drier, and the FT-IR spectrum between a wavenumber of 1500–2000 cm^{-1} was collected with a Nicolet 6700 spectrometer (Thermo Scientific Inc., USA).

Fibrillization of Proteins. Genes encoding WT or mutant HS proteins were synthesized by GenScript Biotech Corporation (Nanjing, China) and constructed into the pQE30 plasmid. Proteins were conventionally expressed in *E. coli* and dissolved in PBS to the concentration of 0.6 mg/mL, stored at $-80\text{ }^\circ\text{C}$ before use. Before fibrillization, protein solutions were passed through 0.22 μm filters to remove possible preformed aggregation. To induce amyloid aggregation of the proteins, the solutions were vigorously agitated (2000 rpm) at $37\text{ }^\circ\text{C}$ for 5 days. To test the seeding effect of preformed aggregates of HS14-19, HS66-71, and HS87-92, peptide stock solutions (5 mM) were diluted to 1 mM and added into WT protein solutions at a volume ratio of 1:100 before agitation. For each sample, ThT-binding fluorescence was measured daily, and mature fibrils formed on day 5 were used for TEM observation and the cytotoxicity assay.

Measurement of Pyrene-Binding Fluorescence. The pyrene crystal was dissolved in dimethyl sulfoxide as 2 mM stock solution. In 500 μL of each peptide sample or PBS as the control, 1 μL of pyrene stock solution was added, and the mixture was incubated at RT for 5 min. A Fluorolog spectrometer was used to measure the fluorescence spectra between 360 and 440 nm using an excitation wavelength of 336 nm. The I_1/I_3 value was calculated as the ratio between the first peak around 371 nm and the third peak around 380 nm. Each peptide was measured for three times, and the averaged I_1/I_3 value was obtained.

Measurement of ANS-Binding Fluorescence. ANS powder was dissolve in PBS as stock solution with concentration of 2 mM. To measure the ANS-binding fluorescence, 500 μL of each peptide sample or PBS as control was mixed with 5 μL of ANS stock solution, and the mixture was incubated at RT for 5 min. Fluorescence spectra between 400 and 600 nm were collected using a Fluorolog spectrometer with excitation wavelength of 350 nm.

Detection of Amyloid Aggregation in the PBS-THF Mixture. Peptide stock solution (5 mM) in PBS was diluted to 1 mM in PBS containing THF with different concentrations ranging from 0 to 40% (v/v). All peptide samples were incubated at RT for 12 h, and ThT-binding fluorescence were

measured. For each peptide, all peak values around 495 nm were normalized as the percentage of the peak value in PBS without THF. To test the effect of THF on preformed fibrils by HS, 0.6 mg/mL WT protein solution was agitated for 5 days and then diluted to 0.3 mg/mL in PBS containing THF with different concentrations ranging from 0 to 40% (v/v). All protein samples were incubated at RT for 12 h, and ThT-binding fluorescence were measured.

Cytotoxicity Assay. PC12 cells purchased from American Type Culture Collection (ATCC, Manassas, VA, USA) were conventionally cultured in the RPMI 1640 medium supplemented with 15% fetal bovine serum. For cytotoxicity assay, cells were seeded in a 96-well plate at a density of 5×10^3 cells per well and incubated for 24 h. After that the medium was replaced with 200 μL of fresh medium containing 20 μL of fibrillized protein or PBS as the control. After 48 h of incubation, cell viability in each well was tested using an Enhanced Cell Counting Kit-8 (Sunbao Biotech, Shanghai, China) following the manufacture's instruction. The optical density (OD) values were detected at 490 nm by a microplate spectrophotometer (BioTek Eon, BioTek Instruments Inc., Winooski, Vermont, USA). Cell viability was calculated as followed

$$\text{Viability}(\%) = \frac{\text{ODp} - \text{ODb}}{\text{ODc} - \text{ODb}} \times 100$$

where ODp was the value of protein samples, ODc was the value of PBS control, and ODb was the value of cell-free medium as blank. Data were the mean values of four repeats and were compared by analysis of variance.

■ ASSOCIATED CONTENT

Supporting Information

The Supporting Information is available free of charge at <https://pubs.acs.org/doi/10.1021/acsomega.0c00979>.

List of experimentally confirmed natural amyloid peptides containing CHAA fragments and comparison of the peak ThT-fluorescent value of different peptides (PDF)

■ AUTHOR INFORMATION

Corresponding Author

Feng Qiu – Laboratory of Anesthesia and Critical Care Medicine, Translational Neuroscience Center and National Clinical Research Center for Geriatrics, West China Hospital and Department of Anesthesiology, West China Hospital, Sichuan University, Chengdu 610041, China; orcid.org/0000-0002-0450-229X; Email: fengqiu@scu.edu.cn

Authors

Yongzhu Chen – Laboratory of Anesthesia and Critical Care Medicine, Translational Neuroscience Center and National Clinical Research Center for Geriatrics, West China Hospital and Periodical Press of West China Hospital, Sichuan University, Chengdu 610041, China

Fei Peng – Laboratory of Anesthesia and Critical Care Medicine, Translational Neuroscience Center and National Clinical Research Center for Geriatrics, West China Hospital and Department of Anesthesiology, West China Hospital, Sichuan University, Chengdu 610041, China

Tao Su – West China-Washington Mitochondria and Metabolism Research Center, West China Hospital, Sichuan University, Chengdu 610041, China

Hao Yang – Key Lab of Transplant Engineering and Immunology, MOH, West China Hospital, Sichuan University, Chengdu 610041, China; orcid.org/0000-0003-2214-9474

Complete contact information is available at:

<https://pubs.acs.org/10.1021/acsomega.0c00979>

Notes

The authors declare no competing financial interest.

ACKNOWLEDGMENTS

This work was financially supported by the National Clinical Research Center for Geriatrics, West China Hospital, Sichuan University (Z2018B21) and the National Natural Science Foundation of China (nos. 81000658 and 31100565).

REFERENCES

- (1) Landreh, M.; Sawaya, M. R.; Hipp, M. S.; Eisenberg, D. S.; Wüthrich, K.; Hartl, F. U. The formation, function and regulation of amyloids: insights from structural biology. *J. Intern. Med.* **2016**, *280*, 164–176.
- (2) Chiti, F.; Dobson, C. M. Protein misfolding, amyloid formation, and human disease: a summary of progress over the last decade. *Annu. Rev. Biochem.* **2017**, *86*, 27–68.
- (3) Iadanza, M. G.; Jackson, M. P.; Hewitt, E. W.; Ranson, N. A.; Radford, S. E. A new era for understanding amyloid structures and disease. *Nat. Rev. Mol. Cell Biol.* **2018**, *19*, 755–773.
- (4) Van Gerven, N.; Van der Verren, S. E.; Reiter, D. M.; Remaut, H. The role of functional amyloids in bacterial virulence. *J. Mol. Biol.* **2018**, *430*, 3657–3684.
- (5) Ke, P. C.; Sani, M.-A.; Ding, F.; Kakinen, A.; Javed, I.; Separovic, F.; Davis, T. P.; Mezzenga, R. Implications of peptide assemblies in amyloid diseases. *Chem. Soc. Rev.* **2017**, *46*, 6492–6531.
- (6) Louros, N. N.; Ionomidou, V. A. Identification of an amyloid fibril forming segment of human Pmel17 repeat domain (RPT domain). *Biopolymers* **2016**, *106*, 133–139.
- (7) Lara, C.; Reynolds, N. P.; Berryman, J. T.; Xu, A.; Zhang, A.; Mezzenga, R. ILQINS hexapeptide, identified in lysozyme left-handed helical ribbons and nanotubes, forms right-handed helical ribbons and crystals. *J. Am. Chem. Soc.* **2014**, *136*, 4732–4739.
- (8) Wong, Y. Q.; Binger, K. J.; Howlett, G. J.; Griffin, M. D. W. Identification of an amyloid fibril forming peptide comprising residues 46–59 of apolipoprotein A-I. *FEBS Lett.* **2012**, *586*, 1754–1758.
- (9) Chaudhary, N.; Nagaraj, R. Self-Assembly of short amyloidogenic peptides at the air-water interface. *Colloid Interface Sci.* **2011**, *360*, 139–147.
- (10) Chen, J.; Ren, R.; Tan, S.; Zhang, W.; Zhang, X.; Yu, F.; Xun, T.; Jiang, S.; Liu, S.; Li, L. A peptide derived from the HIV-1 gp120 coreceptor-binding region promotes formation of PAP248-286 amyloid fibrils to enhance HIV-1 infection. *PLoS One* **2015**, *10*, No. e0144522.
- (11) Frousios, K. K.; Ionomidou, V. A.; Karletidi, C.-M.; Hamdrakas, S. J. Amyloidogenic determinants are usually not buried. *BMC Struct. Biol.* **2009**, *9*, 44.
- (12) Conchillo-Solé, O.; de Groot, N. S.; Avilés, F. X.; Vendrell, J.; Daura, X.; Ventura, S. AGGRESCAN: a server for the prediction and evaluation of “hot spots” of aggregation in polypeptides. *BMC Bioinf.* **2007**, *8*, 65.
- (13) Sivanesan, K.; Andersen, N. Pre-structured hydrophobic peptide β -strands: A universal amyloid trap? *Arch. Biochem. Biophys.* **2019**, *664*, 51–61.
- (14) Qiu, F.; Tang, C.; Chen, Y. Amyloid-like aggregation of designer bolaamphiphilic peptides: effect of hydrophobic section and hydrophilic heads. *J. Pept. Sci.* **2018**, *24*, No. e3062.
- (15) Chen, Y.; Tang, C.; Xing, Z.; Zhang, J.; Qiu, F. Ethanol induced the formation of β -sheet and amyloid-like fibrils by surfactant-like peptide A6K. *J. Pept. Sci.* **2013**, *19*, 708–716.
- (16) Krone, M. G.; Hua, L.; Soto, P.; Zhou, R.; Berne, B. J.; Shea, J.-E. Role of water in mediating the assembly of Alzheimer amyloid-beta A β 16-22 protofilaments. *J. Am. Chem. Soc.* **2008**, *130*, 11066–11072.
- (17) Xie, L.; Luo, Y.; Wei, G. A β (16-22) peptides can assemble into ordered β -barrels and bilayer β -sheets, while substitution of phenylalanine 19 by tryptophan increases the population of disordered aggregates. *J. Phys. Chem. B* **2013**, *117*, 10149–10160.
- (18) Wang, X.; Weber, J. K.; Liu, L.; Dong, M.; Zhou, R.; Li, J. A novel form of β -strand assembly observed in A β (33-42) adsorbed onto graphene. *Nanoscale* **2015**, *7*, 15341–15348.
- (19) Guo, J.; Zhang, Y.; Ning, L.; Jiao, P.; Liu, H.; Yao, X. Stabilities and structures of islet amyloid polypeptide (IAPP22-28) oligomers: from dimer to 16-mer. *Biochim. Biophys. Acta* **2014**, *1840*, 357–366.
- (20) Milardi, D.; Sciacca, M. F. M.; Pappalardo, M.; Grasso, D. M.; La Rosa, C. The role of aromatic side-chains in amyloid growth and membrane interaction of the islet amyloid polypeptide fragment LANFLVH. *Eur. Biophys. J.* **2011**, *40*, 1–12.
- (21) Elias, A. K.; Scanlon, D.; Musgrave, I. F.; Carver, J. A. SEVI, the semen enhancer of HIV infection along with fragments from its central region, form amyloid fibrils that are toxic to neuronal cells. *Biochim. Biophys. Acta* **2014**, *1844*, 1591–1598.
- (22) Al-Mansoori, K.; Hasan, M.; Al-Hayani, A.; El-Agnaf, O. The role of α -synuclein in neurodegenerative diseases: from molecular pathways in disease to therapeutic approaches. *Curr. Alzheimer Res.* **2013**, *10*, 559–568.
- (23) Goedert, M. Alpha-synuclein and neurodegenerative diseases. *Nat. Rev. Neurosci.* **2001**, *2*, 492–501.
- (24) Breydo, L.; Wu, J. W.; Uversky, V. N. α -Synuclein misfolding and Parkinson's disease. *Biochim. Biophys. Acta* **2012**, *1822*, 261–285.
- (25) Eugene, C.; Laghaei, R.; Mousseau, N. Early oligomerization stages for the non-amyloid component of α -synuclein amyloid. *J. Chem. Phys.* **2014**, *141*, 135103.
- (26) Butler, D. C.; Joshi, S. N.; Genst, E. D.; Baghel, A. S.; Dobson, C. M.; Messer, A. Bifunctional anti-non-amyloid component α -synuclein nanobodies are protective in situ. *PLoS One* **2016**, *11*, No. e0165964.
- (27) Morris, K. L.; Zibae, S.; Chen, L.; Goedert, M.; Sikorski, P.; Serpell, L. C. The structure of cross- β tapes and tubes formed by an octapeptide, α S β 1. *Angew. Chem., Int. Ed.* **2013**, *52*, 2279–2283.
- (28) Du, H.-N.; Tang, L.; Luo, X.-Y.; Li, H.-T.; Hu, J.; Zhou, J.-W.; Hu, H.-Y. A peptide motif consisting of glycine, alanine, and valine is required for the fibrillization and cytotoxicity of human alpha-synuclein. *Biochemistry* **2003**, *42*, 8870–8878.
- (29) Giasson, B. I.; Murray, I. V. J.; Trojanowski, J. Q.; Lee, V. M.-Y. A hydrophobic stretch of 12 amino acid residues in the middle of α -synuclein is essential for filament assembly. *J. Biol. Chem.* **2001**, *276*, 2380–2386.
- (30) Carija, A.; Pinheiro, F.; Pujols, J.; Brás, I. C.; Lázaro, D. F.; Santambrogio, C.; Grandori, R.; Outeiro, T. F.; Navarro, S.; Ventura, S. Biasing the native α -synuclein conformational ensemble towards compact states abolishes aggregation and neurotoxicity. *Redox Biol.* **2019**, *22*, 101135.
- (31) Kam, T.-I.; Mao, X.; Park, H.; Chou, S.-C.; Karuppagounder, S. S.; Umanah, G. E.; Yun, S. P.; Brahmachari, S.; Panicker, N.; Chen, R.; et al. Poly(ADP-ribose) drives pathologic α -synuclein neurodegeneration in Parkinson's disease. *Science* **2018**, *362*, No. eaat8407.
- (32) Kyte, J.; Doolittle, R. F. A simple method for displaying the hydrophobic character of a protein. *J. Mol. Biol.* **1982**, *157*, 105–132.
- (33) Sulatskaya, A. I.; Rodina, N. P.; Polyakov, D. S.; Sulatsky, M. I.; Artamonova, T. O.; Khodorkovskii, M. A.; Shavlovsky, M. M.; Kuznetsova, I. M.; Turoverov, K. K. Structural features of amyloid fibrils formed from the full-length and truncated forms of beta-2-microglobulin probed by fluorescent dye thioflavin T. *Int. J. Mol. Sci.* **2018**, *19*, 2762.

(34) Sulatskaya, A. I.; Rodina, N. P.; Sulatsky, M. I.; Povarova, O. I.; Antifeeva, I. A.; Kuznetsova, I. M.; Turoverov, K. K. Investigation of α -synuclein amyloid fibrils using the fluorescent probe thioflavin T. *Int. J. Mol. Sci.* **2018**, *19*, 2486.

(35) Martial, B.; Lefèvre, T.; Buffeteau, T.; Auger, M. Vibrational circular dichroism reveals supramolecular chirality inversion of α -synuclein peptide assemblies upon interactions with anionic membranes. *ACS Nano* **2019**, *13*, 3232–3242.

(36) Okada, Y.; Okubo, K.; Ikeda, K.; Yano, Y.; Hoshino, M.; Hayashi, Y.; Kiso, Y.; Itoh-Watanabe, H.; Naito, A.; Matsuzaki, K. Toxic amyloid tape: a novel mixed antiparallel/parallel β -sheet structure formed by amyloid β -protein on GM1 clusters. *ACS Chem. Neurosci.* **2019**, *10*, 563–572.

(37) Taylor, D. L.; Allen, R. D.; Benditt, E. P. Determination of the polarization optical properties of the amyloid-Congo red complex by phase modulation microspectrophotometry. *J. Histochem. Cytochem.* **1974**, *22*, 1105–1112.

(38) Surewicz, W. K.; Mantsch, H. H.; Chapman, D. Determination of protein secondary structure by Fourier transform infrared spectroscopy: a critical assessment. *Biochemistry* **1993**, *32*, 389–394.

(39) Barth, A.; Zscherp, C. What vibrations tell us about proteins. *Q. Rev. Biophys.* **2002**, *35*, 369–430.

(40) Xu, F.; Liu, J.; Tian, J.; Gao, L.; Cheng, X.; Pan, Y.; Sun, Z.; Li, X. Supramolecular self-assemblies with nanoscale RGD clusters promote cell growth and intracellular drug delivery. *ACS Appl. Mater. Interfaces* **2016**, *8*, 29906–29914.

(41) Shu, C.; Sabi-mouka, E. M. B.; Wang, X.; Ding, L. Self-assembly hydrogels as multifunctional drug delivery of paclitaxel for synergistic tumour-targeting and biocompatibility in vitro and in vivo. *J. Pharm. Pharmacol.* **2017**, *69*, 967–977.

(42) Huang, Z.-H.; Shi, L.; Ma, J.-W.; Sun, Z.-Y.; Cai, H.; Chen, Y.-X.; Zhao, Y.-F.; Li, Y.-M. A totally synthetic, self-assembling, adjuvant-free MUC1 glycopeptide vaccine for cancer therapy. *J. Am. Chem. Soc.* **2012**, *134*, 8730–8733.

(43) Rad-Malekshahi, M.; Fransen, M. F.; Krawczyk, M.; Mansourian, M.; Bourajaj, M.; Chen, J.; Ossendorp, F.; Hennink, W. E.; Mastrobattista, E.; Amidi, M. Self-assembling peptide epitopes as novel platform for anticancer vaccination. *Mol. Pharmaceutics* **2017**, *14*, 1482–1493.

(44) Wang, S.-T.; Lin, Y.; Spencer, R. K.; Thomas, M. R.; Nguyen, A. I.; Amdursky, N.; Pashuck, E. T.; Skaalure, S. C.; Song, C. Y.; Parmar, P. A.; Morgan, R. M.; Ercius, P.; Aloni, S.; Zuckermann, R. N.; Stevens, M. M. Sequence-dependent self-assembly and structural diversity of islet amyloid polypeptide-derived β -sheet fibrils. *ACS Nano* **2017**, *11*, 8579–8589.

(45) Xu, H.; Wang, J.; Han, S.; Wang, J.; Yu, D.; Zhang, H.; Xia, D.; Zhao, X.; Waigh, T. A.; Lu, J. R. Hydrophobic-region-induced transitions in self-assembled peptide nanostructures. *Langmuir* **2009**, *25*, 4115–4123.

(46) Fadnavis, N. W.; Seshadri, R.; Sheelu, G.; Madhuri, K. V. Relevance of Frank's solvent classification as typically aqueous and typically non-aqueous to activities of firefly luciferase, alcohol dehydrogenase, and alpha-chymotrypsin in aqueous binaries. *Arch. Biochem. Biophys.* **2005**, *433*, 454–465.

(47) Mandal, P.; Molla, A. R. Solvent Perturbation of Protein Structures - A Review Study with Lectins. *Protein Pept. Lett.* **2019**, *26*, 1.